electronics

Article

Novel Nth/2Nth Order Two-Band Bandpass Filters for Sub-6 GHz 5G Applications

Ceyhun Karpuz [1,*], Pınar Öztürk Özdemir [2] and Gülfem Balasu Fırat Unuk [1]

[1] Department of Electrical and Electronics Engineering, Pamukkale University, 20160 Denizli, Turkey
[2] Air Force Academy, National Defence University, 34149 Istanbul, Turkey
* Correspondence: ckarpuz@pau.edu.tr

Abstract: In this paper, a new design method is proposed for multi-mode two-band bandpass filters based on combining a square loop resonator that has a capacitive perturbation element and short-circuited stubs. This concept is a new multi-mode two-band filter design having Nth and 2Nth order for the first and second passbands that appear in f_0 and $3f_0$ center frequencies, respectively. It has been shown that the number of transmission modes in each passband can easily be increased by periodically cascading one unit filter cell including one square loop resonator and two short-circuited stubs. This also provides a reconfigurable filter property, namely the obtaining of two different filtering characteristics in the second passband by means of the reverse and straight placing of the cascaded unit filter cells in the horizontal axis. Two 2nd/4th order two-band bandpass filter prototypes are fabricated and tested to validate the proposed design method. The total surface areas of these fabricated prototypes are 26.0 mm × 9.0 mm and 24.4 mm × 16.8 mm, and the measured insertion losses in the first/second passband are about 0.63 dB/0.96 dB and 0.59 dB/0.83 dB. It is observed that the filter prototypes have the advantages of low insertion loss, compact size, and flexible filtering characteristics. The designed filters are suitable for operation in the 5G spectrum, which includes a range of radio frequencies sub-6 GHz.

Keywords: two-band filter; perturbation element; short-circuited stub; square loop resonator

Citation: Karpuz, C.; Özdemir, P.Ö.; Unuk, G.B.F. Novel Nth/2Nth Order Two-Band Bandpass Filters for Sub-6 GHz 5G Applications. *Electronics* **2023**, *12*, 626. https://doi.org/10.3390/electronics12030626

Academic Editor: Alejandro Melcón Alvarez

Received: 9 January 2023
Revised: 19 January 2023
Accepted: 25 January 2023
Published: 27 January 2023

1. Introduction

The requirement for multiband microwave filters with high performance increases by the day due to the rapid developments in modern multifunction communication systems. Among these filters, two-band filters are highly desired. Microstrip structures are the essential components in the design of two-band filters due to the merits of high selectivity, design flexibility and compact size. A dual-mode microstrip resonator is a good candidate to improve the selectivity and reduce the size for designing two-band bandpass filters. To date, many two-band bandpass filters have been developed using various methods. One of the most direct methods to design a two-band bandpass filter is to combine two single-band bandpass filters that have different passbands [1]. This method enables the design of high-performance two-band filters with controllable center frequencies, order, and transmission zeros; however, such designs suffer from a large surface area. Another effective way to achieve a two-band filter is to cascade a bandpass filter and a bandstop filter [2]. In this method, isolation between the two passbands may be a problem. Usually, it is widely preferred to design two-band filters in virtue of the first two resonance frequencies of SIR [3–5], stub [6–8], patch [9] and loop resonators [10,11].

This paper discusses a design method of a multi-mode bandpass filter having two passbands at approximately f_0 and $3f_0$ center frequencies. The proposed design method is analyzed by a theoretical approach based on even-odd mode analysis and ABCD parameters. The main goal of the method is to design two-band filters having the first/second passband with Nth/2Nth order by using N sequential cascaded unit filter cells. Each unit

filter cell is formed by a capacitively loaded square loop resonator and short-circuited stubs located along the transmission line directly connected to I/O ports. The capacitively-loaded square loop resonator creates a dual-mode wide-passband and the short-circuit stubs are used to obtain the bandpass characteristic from the lowpass characteristic in the first band. For demonstration, two dual-mode two-band filters with different design concepts are implemented using two cascaded unit filter cells. These concepts ensure that the first passband characteristic is fixed while the second passband has a linear or elliptical filter characteristic, depending on the placement of the resonators and stubs on the main line. Compared with our previous study [12], square loop resonators are used instead of patch resonators with the same surface area in the proposed design. It is noted that using the square loop resonator leads to significant miniaturization in the second passband.

2. Analysis of the Proposed Unit Filter Cell

It is well known that open-circuit and short-circuited stubs act as series and parallel resonance circuits, respectively. Therefore, such stubs can be used along a transmission line in bandpass and bandstop filter design. The characteristic impedance, the electrical length, and the connecting point of the stubs are critical parameters for filter designs using open/short-circuited stubs. The equivalent circuit models for bandpass and bandstop filter circuits, which can be obtained when the transmission line and stub are used with a length of $\lambda/4$ at the center frequency, are well-described in the literature [13,14]. As depicted in Figure 1b,c and Figure 2b,c, the transmission line (TL) and lumped element (LE) equivalent circuit models based on the line parameters and the element values are used to derive design equations of the bandstop and the bandpass filter characteristic. One method to obtain a wide passband in the design of bandpass filters is using resonators directly connected to I/O ports, as illustrated in Figure 3. As is well known from dual-mode resonator theory, the degenerate modes are excited by the perturbation effect that can be achieved by locating and cutting a small patch at the symmetry axis of the resonator [15,16]. This effect can also be achieved by using a thin film capacitor instead of a patch perturbation element. Therefore, to obtain a dual mode in the wide passband, a resonator is used in which a thin film capacitor is placed in the middle of the upper path, which is located on the opposite side of the I/O ports. Figure 4 shows the topology of the square loop resonator with a thin film capacitor employed as a perturbation element. The capacitor that creates a perturbation effect is located on the symmetrical axis in the upper arm of the resonator to create mode splitting. The value of this capacitor can be calculated by using even-odd mode analysis depending on the desired return loss level in the passband.

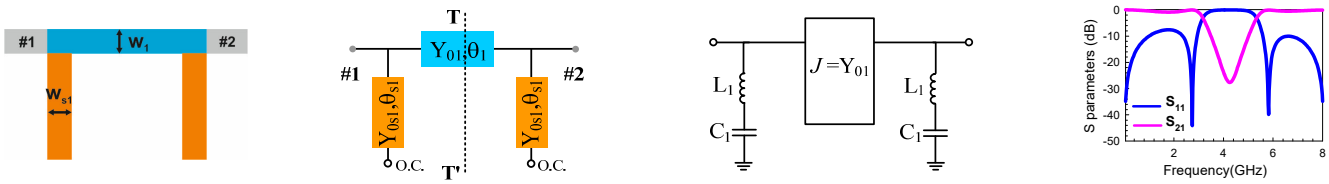

Figure 1. (**a**) A bandstop filter circuit with open-circuit stubs (**b**) TL model (**c**) LE model (**d**) frequency response.

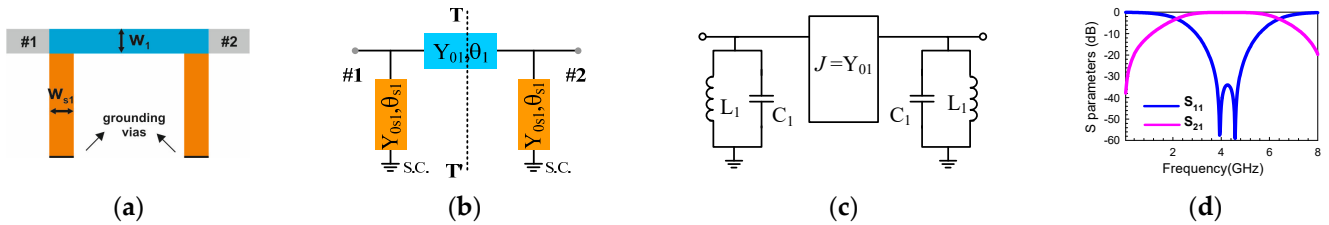

Figure 2. (**a**) A bandpass filter circuit with short-circuited stubs (**b**) TL model (**c**) LE model (**d**) frequency response.

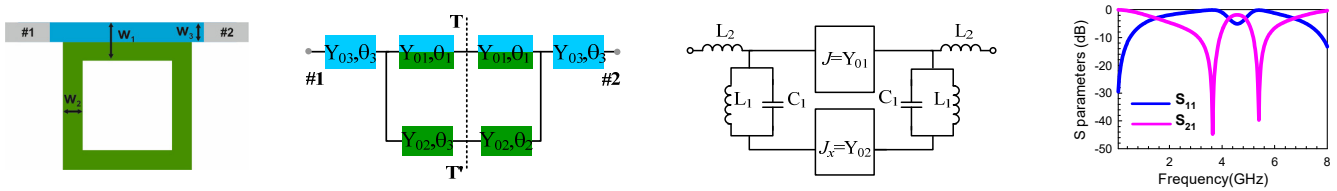

Figure 3. (**a**) A bandpass filter circuit by using square loop resonator (**b**) TL model (**c**) LE model (**d**) frequency response.

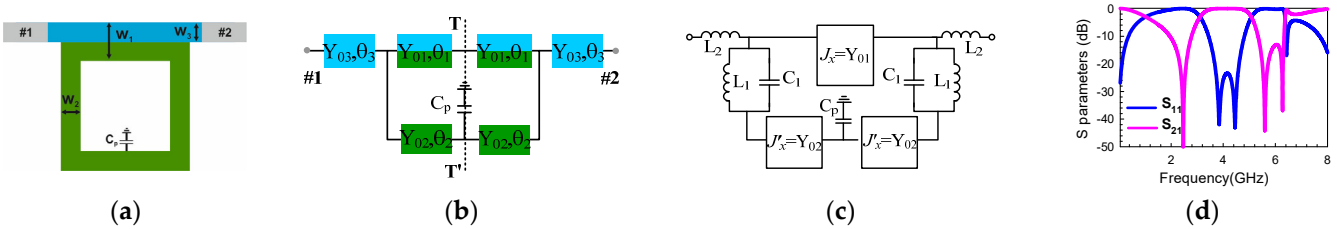

Figure 4. (**a**) A bandpass filter circuit by using a square loop resonator with perturbation element (**b**) TL model (**c**) LE model (**d**) frequency response.

Figures 5 and 6 show the geometry formed by the combination of the stubs and square loop resonator, which is located on a main transmission line connecting the I/O ports. It should be noted that the circuits are symmetrical according to the TT′ plane. Such configurations are called unit filter cells in this paper. Figures 5a and 6a show the two different topologies of the unit filter cell. TE and LE equivalent circuits corresponding to these topologies are given in Figures 5b, 6b and 5c, Figure 6c, respectively. The frequency responses of the unit filter cells are shown in Figures 5d and 6d. Accordingly, a multi-mode two-band bandpass filter may be designed by using the unit cell configuration having the two-band characteristic given in Figure 6a. Even-odd mode analysis, which is a widely used method in the literature [17,18], is performed for the unit filter cell to describe the design method of the two-band bandpass filter. For this purpose, the unit filter cell having the two-band characteristic given in Figure 6a is first analyzed through even-odd mode impedance analysis. Due to the reciprocal topology, even-odd mode analysis can be used on the symmetry plane TT′ to investigate the behavior of the unit cell. The TL and LE equivalent circuit models of the proposed unit filter cell are illustrated in Figures 6b and 6c, respectively. To analyze the circuit, even- and odd-mode half circuits can be obtained by placing magnetic and electric walls to the symmetry axis TT′ in the TL model, respectively. Thus, the symmetry axis must be open- and short-circuited for the even and odd modes, as illustrated in Figures 7a and 7b, respectively.

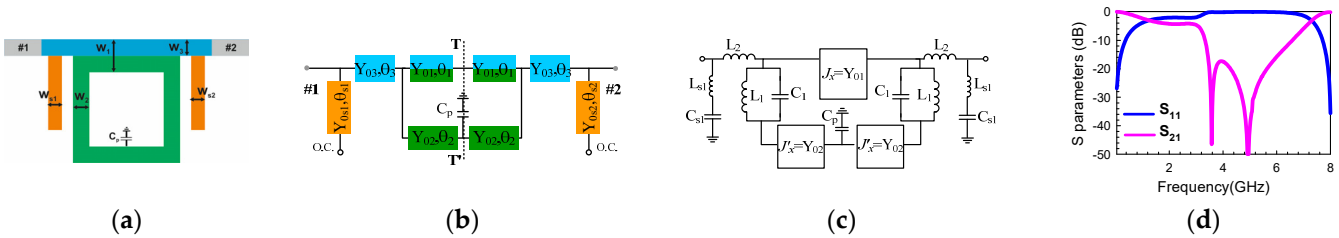

Figure 5. (**a**) A bandstop filter circuit by using a square loop resonator with perturbation element and open-circuited stubs (**b**) TL model (**c**) LE model (**d**) frequency response.

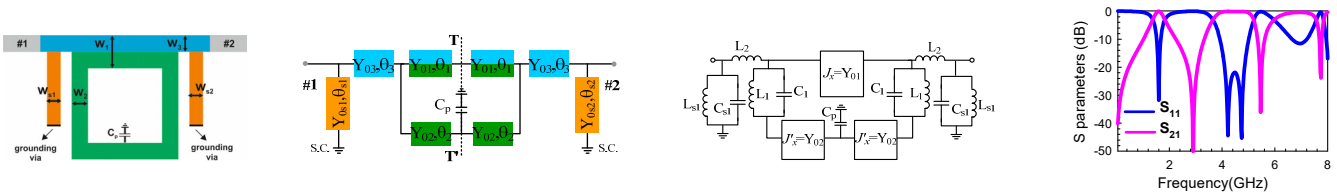

(**a**) (**b**) (**c**) (**d**)

Figure 6. (**a**) A bandpass filter circuit by using a square loop resonator with perturbation element and short-circuited stubs (**b**) TL model (**c**) LE model (**d**) frequency response.

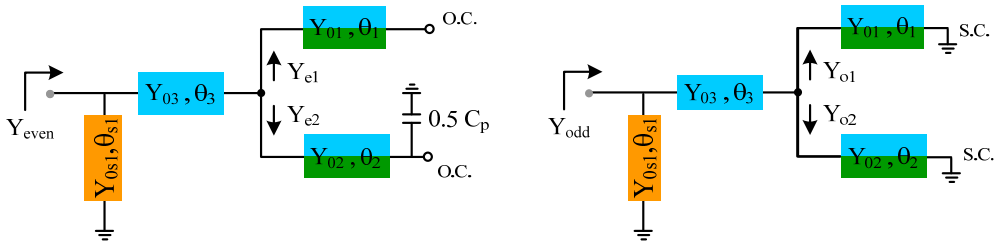

(**a**) (**b**)

Figure 7. (**a**) Even- (**b**) odd-mode half circuit TL models of the unit filter cell.

Even- and odd-mode input admittances ($Y_{even/odd}$) can be calculated by,

$$Y_{even/odd} = -jY_{0s1}\cot(\theta_{s1}) + Y_{03}\frac{(Y_{e1/o1} + Y_{e2/o2}) + jY_{03}\tan(\theta_3)}{Y_{03} + j(Y_{e1/o1} + Y_{e2/o2})\tan(\theta_3)} \quad (1)$$

where the electrical lengths of θ_1 and θ_2 are related to the top and bottom lines of the resonator, and their characteristic admittances are called Y_{01} and Y_{02}, respectively. θ_3 represents the electrical length of the transmission line with characteristic admittance Y_{03}. θ_{s1} is the electrical length of the short-circuited stub and Y_{0s1} is the characteristic impedance of this stub. $Y_{e1/o1}$ and $Y_{e2/o2}$ are the admittances seen from the input of the top and bottom paths of the half circuit of the resonator under even- and odd-mode excitation, respectively. For even-mode excitation, these admittances are expressed by,

$$Y_{e1} = jY_{01}\tan(\theta_1), \quad (2)$$

$$Y_{e2} = Y_{02}\frac{jb_p + jY_{02}\tan(\theta_2)}{Y_{02} - b_p\tan(\theta_2)} \quad (3)$$

where b_p describes the susceptance of perturbation capacitance and can be represented by $0.5wC_p$. Similarly, the odd-mode input admittances for both paths can be defined by means of

$$Y_{o1} = -jY_{01}\cot(\theta_1), \quad (4)$$

$$Y_{o2} = -jY_{02}\cot(\theta_2). \quad (5)$$

In this case, the even- and odd-mode resonance conditions can be obtained by setting the imaginary parts of the even- and odd-mode input admittances ($Y_{even/odd}$) to zero. According to Equations (4) and (5), the perturbation capacitance (C_p) is only situated in the even-mode half-circuit and as can be seen from these equations, it only affects the even-mode frequency. It should be also noted that the resonance conditions for even and odd modes can be revised when short-circuited stubs are not used in the circuit so that the sum of the input admittances of the half resonator circuit equals zero. In this case, the

resulting scattering parameters for two configurations seen in Figures 4a and 6a can be obtained by using the even/odd-mode input admittances as follows [14];

$$S_{11} = \frac{Y_0^2 - Y_{even}Y_{odd}}{(Y_0 + Y_{even})(Y_0 + Y_{odd})}, \tag{6}$$

$$S_{21} = \frac{Y_0Y_{odd} - Y_0Y_{even}}{(Y_0 + Y_{even})(Y_0 + Y_{odd})}. \tag{7}$$

From (7), it is clear that the transmission zeros are exhibited in case the odd-mode input admittance is equal to that of the even mode. In this case, the transmission zeros appear closely related to the capacitance used as the perturbation element. The calculated frequency responses are compared in Figure 8. In this case, the first and second passband having the single and dual modes is located at approximately f_0 and $3f_0$ center frequencies through a unit filter section.

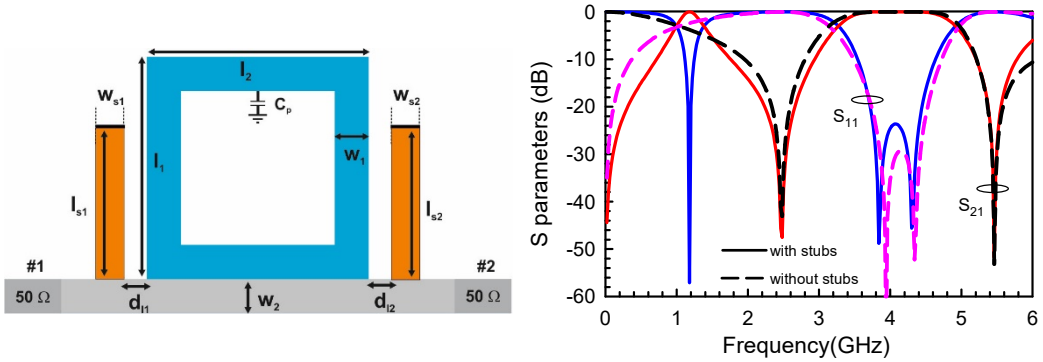

(**a**) (**b**)

Figure 8. (**a**) Configuration of the unit filter cell (**b**) Comparison of calculated S parameters with/without short-circuited stubs.

By adding short-circuited stubs to the resonator, there is a transformation from lowpass to bandpass characteristic in the first passband, as can be seen from Figure 8b. In contrast, no significant change is observed in the characteristic of the second passband since it is based on the configuration of the resonator, as can be seen from Figure 8b. It is clearly observed that the mode frequencies of the second passband can be controlled by the resonator dimensions and the value of the perturbation element from this comparison. The dimensions of this structure are $l_1 = l_2 = 7.8$, $w_1 = w_2 = 1.2$, $l_{s1} = l_{s2} = 7.0$, $w_{s1} = w_{s2} = 0.8$, $d_{s1} = d_{s2} = 2.0$ (all units in mm). Figure 9 shows the effect in the second passband due to the change in the perturbation capacitance (C_p) on the square loop resonator in the unit filter cell. As can be observed from Figure 9, the modes are split when the perturbation capacitance is about 1.1 pF. The frequencies of degenerate modes for the second passband are marked as f_1 (for even mode) and f_2 (for odd mode) in Figure 9. According to Equations (2)–(5), only one mode is affected by the perturbation capacitance. Therefore, the variation in the C_p capacitance changes the frequency of the even mode (f_1) while the frequency of the odd mode (f_2) remains almost fixed. As a consequence, the bandwidth varies rapidly on the left side while little change is observed on the right side since the even-mode frequency is lower than the odd-mode frequency ($f_1 < f_2$). The frequencies of the transmission zeros are represented by f_{tz1} and f_{tz2} in Figure 9. It is also seen from the figure that transmission zero on the left side of the passband moves faster than the right side and the passband exhibits more asymmetric behavior depending on the increment in C_p.

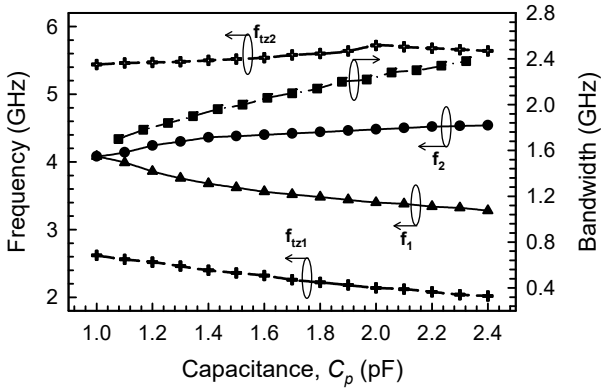

Figure 9. Mode (f_1 and f_2) and transmission zero (f_{tz1} and f_{tz2}) frequencies and bandwidth variation depending on C_p.

3. Design Method for Nth/2Nth Order Two-Band Bandpass Filter

The design methodology is based on the configuration of the unit filter cell introduced in Section 2. Depending on filter properties such as center frequency of the passbands, bandwidth, return loss or insertion loss level, etc., the first step is to determine the dimension of the square loop resonators based on even-odd mode analysis. A thin film capacitor that creates a perturbation effect is located on the symmetrical axis in the upper paths of the resonator to create mode splitting. The desired value of the capacitor can be adjusted based on the analysis depending on the prescribed properties. After deciding the dimension of the resonator, short-circuited stubs are placed on both sides of the resonator to provide symmetry in the configuration. By adding short-circuited stubs to the resonator, there is a transformation from lowpass to bandpass characteristic in the first passband. In this case, first and second passbands having single and dual modes are obtained using unit filter section. Thus, the proposed design method differs from other studies including conventional filter designs using shunt/series-coupled resonators [19,20] in the respect that it provides a topology that includes a frequency response having Nth/2Nth order first/second passbands located at $f_0/3f_0$ center frequencies.

Figure 10a shows the general topology indicating the physical design parameters of the **Two-Band F**ilter with a **S**quare **L**oop **R**esonator (**TBFSLR**). To increase the number of transmission modes in each passband, each unit filter cell consisting of a square loop resonator, two short-circuited stubs, and transmission lines directly connecting the I/O ports, are cascaded. In this case, it is convenient to use ABCD matrices to obtain a theoretical model for the proposed circuit. As stated in the literature [13], the ABCD matrix exhibits the voltage and current relationship for the two-port network. Since cascade-connected components are used in the design, the ABCD matrix of the unit filter cell can be obtained by multiplying the ABCD matrices of each component. The ABCD matrix of the unit cell can be defined as;

$$\begin{aligned} A_1 = {} & (j2Y_{03}^2(Y_{0s1}\cot\theta_{s1} - Y_{03}\tan\theta_3) - j2\tan\theta_3(Y_{03} + Y_{0s1}\cot\theta_{s1}\tan\theta_3)(Y_{e1} + Y_{e2})(Y_{o1} + Y_{o2}) \\ & -Y_{03}(2Y_{0s1}\cot\theta_{s1}\tan\theta_3 - Y_{03}\tan\theta_3^2 + Y_{03})(Y_{e1} + Y_{e2} + Y_{o1} + Y_{o2}))/Y_{03}^2(\tan\theta_3^2 + 1)(Y_{e1} + Y_{e2} - Y_{o1} - Y_{o2}) \end{aligned} \tag{8a}$$

$$\begin{aligned} B_1 = {} & (2\tan\theta_{03}^2(Y_{e1} + Y_{e2})(Y_{o1} + Y_{o2}) - j2Y_{03}\tan\theta_3(Y_{e1} + Y_{e2} + Y_{o1} + Y_{o2}) - 2Y_{03}^2) \\ & /Y_{03}^2(\tan\theta_3^2 + 1)(Y_{e1} + Y_{e2} - Y_{o1} - Y_{o2}) \end{aligned} \tag{8b}$$

$$\begin{aligned} C_1 = {} & (2Y_{03}^2(Y_{0s1}\cot\theta_{s1} - Y_{03}\tan\theta_{03})^2 - 4(Y_{03} + Y_{0s1}\cot\theta_{s1}\tan^2\theta_{03})(Y_{e1} + Y_{e2})(Y_{o1} + Y_{o2})) \\ & /Y_{03}^2(\tan\theta_3^2 + 1)(Y_{e1} + Y_{e2} - Y_{o1} - Y_{o2}) \end{aligned} \tag{8c}$$

$$\begin{aligned} D_1 = {} & (j2Y_{03}^2(Y_{0s1}\cot\theta_{s1} - Y_{03}\tan\theta_3) - j2\tan\theta_3(Y_{03} + Y_{0s1}\cot\theta_{s1}\tan\theta_3)(Y_{e1} + Y_{e2})(Y_{o1} + Y_{o2}) \\ & -Y_{03}(2Y_{0s1}\cot\theta_{s1}\tan\theta_3 - Y_{03}\tan\theta_3^2 + Y_{03})(Y_{e1} + Y_{e2} + Y_{o1} + Y_{o2}))/Y_{03}^2(\tan\theta_3^2 + 1)(Y_{e1} + Y_{e2} - Y_{o1} - Y_{o2}) \end{aligned} \tag{8d}$$

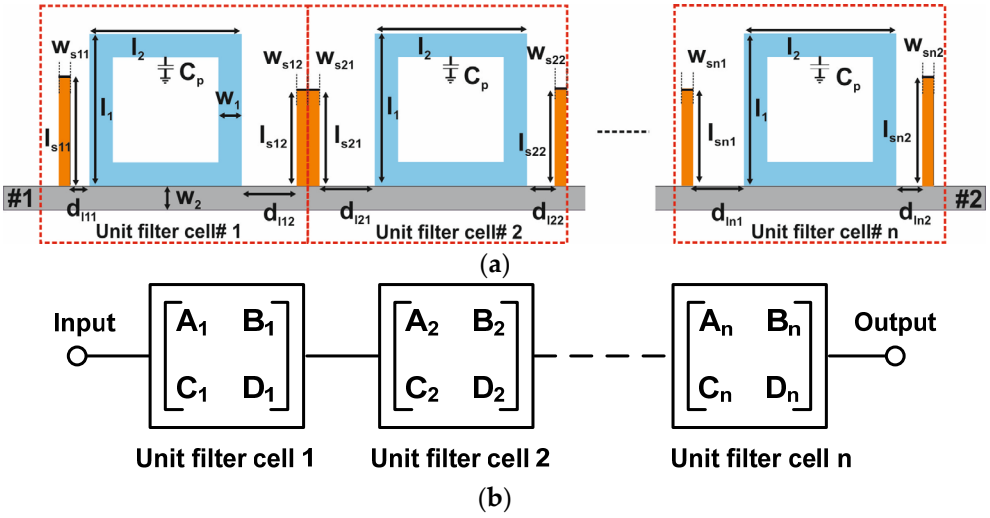

Figure 10. (**a**) General configuration, (**b**) Schematic diagram of the TBFSLR.

In Equation (8), the ABCD parameters of a unit filter cell are given in terms of even- and odd-mode input admittance provided by means of the analysis in Section 2. The even/odd-mode input admittances of the unit filter cell have been converted to the ABCD matrix for the determination of all sections of the proposed two-band filter. Finally, N unit filter cells are periodically connected along a transmission line to create Nth/2Nth order passbands. While the first passband with N degrees is obtained at f_0 (center frequency), the second passband with 2N degrees is located at $3f_0$.

Figure 10a shows the general topology of the two-band filter, which consists of a combination of unit filter cells. As can be seen from the figure, the configuration includes short-circuited stubs placed at a proper distance on both sides of the square loop resonator is used, and the N unit filter cells are periodically connected to create passbands with Nth/2Nth order. The schematic diagram of the proposed two-band filter with a square loop resonator is given in Figure 10b. The filter circuit can be analyzed by defining the related ABCD matrix of all unit filter cells. Therefore, the matrix can be generalized and defined for each unit filter and formulated as

$$\begin{bmatrix} A & B \\ C & D \end{bmatrix} = \prod_{i=1}^{N} \begin{bmatrix} A_i & B_i \\ C_i & D_i \end{bmatrix}. \tag{9}$$

The two-band filter circuit is characterized by the multiplication of the ABCD matrices of each unit cell as given in Equation (9). In order to provide the frequency response of the proposed two-band filter, the ABCD matrix needs to be converted to the S parameters [13].

The circuit design of a two-band bandpass filter with two, triple and quad sections is employed as an example to demonstrate the validity of the theoretical analysis using the ABCD matrix. Each unit cell is composed of the resonator, the short-circuited stubs, and the transmission lines connecting them. The circuits are reciprocally symmetrical with respect to the I/O ports. The dimensions of the two-band filter with 2nd/4th order are given in Table 1 (TBFSLR#1). The distances between the short-circuited stubs and loop resonators are 0.8 mm, 2.3 mm and 4 mm for the 3rd/6th order filter and 0.8 mm, 2.2 mm, 4.2 mm and 3.5 mm for the 4th/8th order filter. The capacities used in the first and last resonators are 1pF, and for the middle resonators, 0.8pF. All other parameters are the same as for the 2nd/4th order filter. The ABCD matrices of all the filters can be arranged by (9). According to these equations, scattering parameters can be obtained by the conventional transformation from the ABCD [14]. The frequency responses extracted from the total ABCD matrix of the filter circuit containing two, triple and quad filter cells are compared with the simulated response in Figure 11. It is clearly seen that the first/second passband

with 2nd/4th, 3rd/6th, and 4th/8th order is obtained in the frequency response as expected for N = 2, 3, and 4, respectively.

Table 1. Dimensions (in mm) of the two-band filters having first/second passband with 2nd/4th order.

	w_1	w_2	w_{s11}	w_{s12}	l_1	l_2	l_{s11}	l_{s12}	d_{l11}	d_{l12}
TBFSLR#1	1.2	1.2	0.4	1.0	7.8	7.8	7.3	5.4	0.8	3.0
TBFSLR#2	1.2	1.2	0.4	0.5	7.8	7.8	7.3	5.9	0.5	3.0

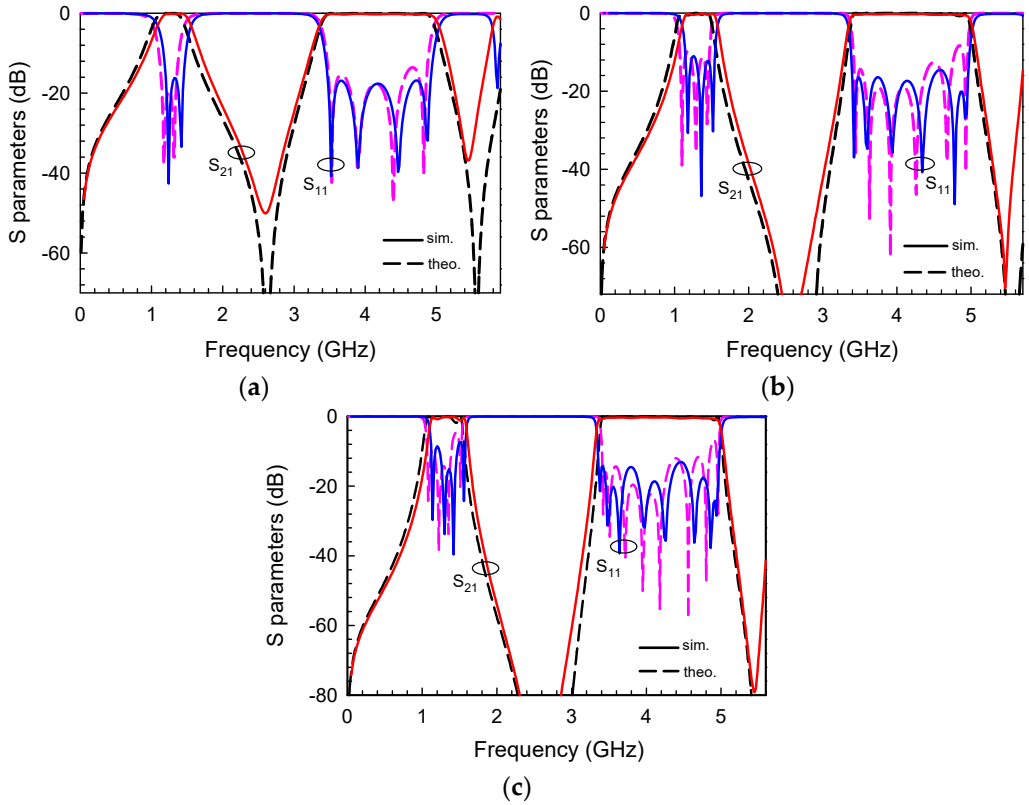

Figure 11. Comparison of the simulated and calculated frequency response for (**a**) N = 2, (**b**) N = 3, (**c**) N = 4.

4. Configuration of Microstrip Nth/2Nth Order Two-Band Bandpass Filter

Based on the analysis in Section 2, the multi-mode two-band filter can be configured by the following design steps.

Step 1—Specify the filter properties such as center frequency of the passbands, bandwidth, return loss or insertion loss level, etc . . .

Step 2—Determine the dimension of the square loop resonators based on the even-odd mode analysis following filter specifications in Step 1.

Step 3—Provide the other passband by using short-circuited stubs placed symmetrically on both sides of the resonator. By adding short-circuited stubs to the resonator, there is a transformation from lowpass to bandpass characteristic in the first passband. In contrast, no significant change is observed in the characteristic of the second passband since it is based on the configuration of the resonator. Thus, the center frequency of the added passband is adjusted by the length and width of the stubs.

Step 4—Place a thin film capacitor in the square loop resonator circuit to duplicate the mode frequencies in the second passband. Hence, the unit filter cell, which is the fundamental building block of the proposed configuration for the two-band filter design in the article, is obtained. A thin film capacitor that creates a perturbation effect is placed on

the symmetrical axis in the upper arm of the resonator. The feature of having a duplicated mode instead of an equal mode on the second passband also distinguishes the proposed structure from conventional filter designs with stubs.

Step 5—Construct the two-band bandpass filter having the N/2N mode obtained by using the cascading arrangement of N unit filter cells.

The cascaded unit filter cells can be straight or inversely connected on the horizontal axis to achieve two different filtering characteristics in the second passband. In the configuration, the distance between the stubs and the resonator and the width of the stubs are chosen so that a uniform equiripple can be obtained, especially in the second passband. The design steps are summarized in the flowchart shown in Figure 12.

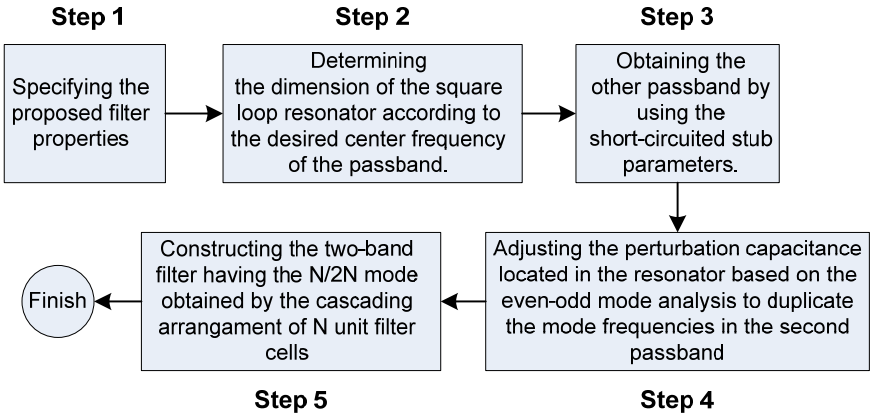

Figure 12. Design steps of the configuration of Nth/2Nth order two-band bandpass filter.

In the design, the square loop resonator has a thin film capacitor and short-circuited stubs placed between the input and output ports to increase modes in each passband. In addition, two different types of two-band filters in terms of the characteristics of the second passband are achieved based on the placement of the loop resonators and short-circuited stubs. The two-band filters having the first/second passband with 2nd/4th order are called TBFSLR#1 and TBFSLR#2. TBFSLR#1 has a flat group delay and a very compact size. While TBFSLR#2 is slightly larger than TBFSLR#1, it provides higher selectivity. The layouts of TBFSLR#1 and TBFSLR#2 are given in Figure 13a.

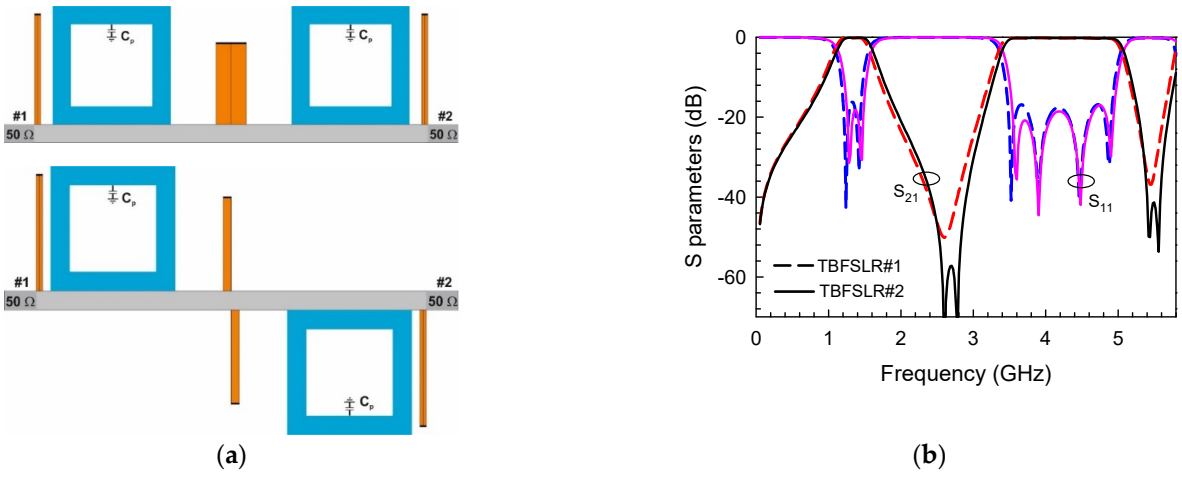

(**a**) (**b**)

Figure 13. The configuration of the (**a**) TBFSLR#1 and TBFSLR#2, (**b**) Comparison of the simulated frequency responses.

The designed filters are configured on a Rogers RT6010LM substrate with a thickness of 1.27 mm and a relative dielectric constant of 10.2. The length and width of the short-circuited stubs have been optimized through EM simulation [21] to achieve the optimum

return loss levels. The *S* parameters of TBFSLR#1 and TBFSLR#2 are shown in Figure 13b. As can be seen from the figure, the transmission modes are duplicated in each passband for both filters. The dimensions of the two-band filters (TBFSLR#1 and TBFSLR#2) are given in Table 1. The values of the perturbation capacitances (C_p) are 1.0 pF in both filters. The C_p value can be chosen so that the desired bandwidth or return loss level is obtained in the second passband. In these configurations, C_p is determined as 1 pF by using even-odd mode analysis to provide a return loss with an equiripple at about −20 dB in the second passband, as can be seen in Figure 13b.

To investigate in detail the effect of circuit parameters on frequency response, TBFSLR#1 has been simulated by using a full-wave electromagnetic simulator [21]. It was found that the effect of the parameters on the frequency response of TBFSLR#1 is similar to the effect on the filter (DBF#1) presented in [12]. C_p can be used to control the second passband of the filter, as observed in Figure 14. The bandwidth of the second passband can be adjusted from the left side of the passband while the bandwidth of the first passband is kept fixed at about 500 MHz. The bandwidth of the second passband increases from 1640 MHz to 1760 MHz as the C_p value changes between 0.9 pF and 1.2 pF. At the same time, the return loss level in the second passband is changing, but it remains almost constant in the first passband, as shown in Figure 14.

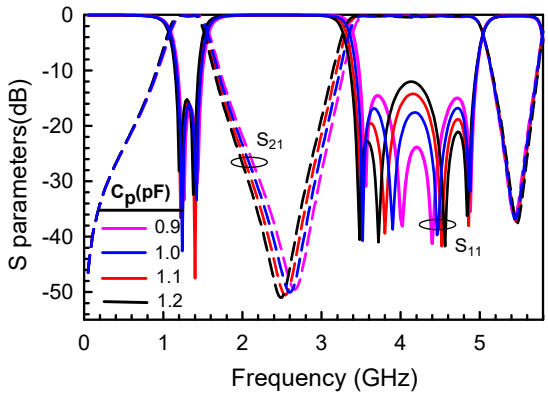

Figure 14. Effect of varying C_p on the frequency response of TBFSLR#1.

The short-circuited stub is effective in determining the first passband. For this reason, changes in short-circuited stubs have more of an effect on the first passband. The bandwidth of the first passband can be controlled by means of the width of the short-circuited stubs (w_{s12}/w_{s21}) between the two square loop resonators. As Figure 15 shows, the bandwidth of the first passband increases from 340 MHz to 560 MHz, while the bandwidth of the second passband remains constant at 1700 MHz, when w_{s12} and w_{s21} simultaneously decrease in width from 1.8 mm to 0.6 mm.

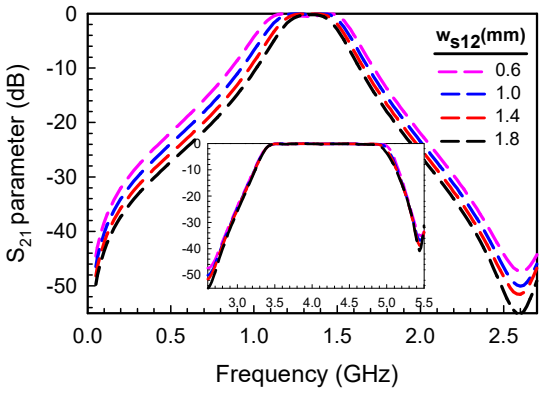

Figure 15. Effect of varying w_{s12} on the bandwidth of the first passband.

The length of the short-circuited stubs is effective in the return loss change of both passbands, as depicted in Figure 16. It is obvious from Figures 14 and 16b that the C_p, l_{s12} and l_{s21} parameters can be changed together to keep the return loss of the second passband at the same level. In this way, the return loss level of the first passband can be controlled by these parameters.

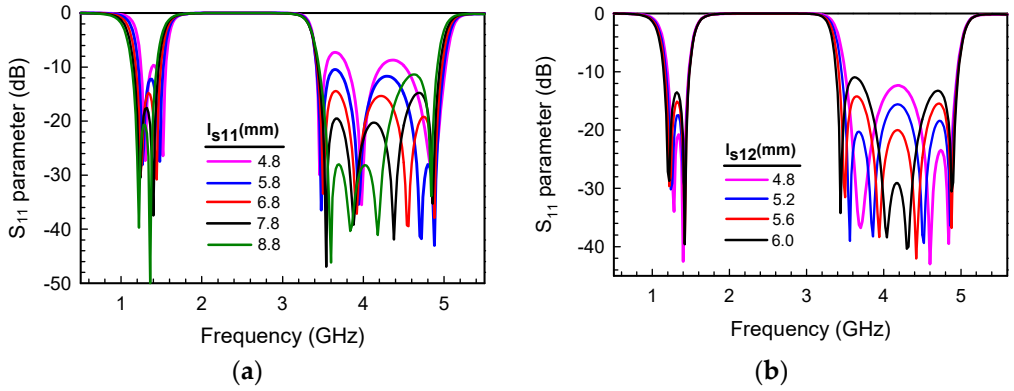

Figure 16. Variation in return loss levels versus different lengths of (**a**) $l_{s11} = l_{s22}$, (**b**) $l_{s12} = l_{s21}$.

The bandwidths of the filter can be controlled on both sides of the passbands by changing the length of the stubs between the resonators ($l_{s12} = l_{s21}$) and distances between the square loop resonator and a short-circuited stub ($d_{l12} = d_{l21}$). When l_{s12} and l_{s21} simultaneously range from 4.2 mm to 6.6 mm, the bandwidths of the first and second passbands increase from 400 MHz to 520 MHz and from 1600 MHz to 1780 MHz, respectively. In this manner, the bandwidth increases from the left side for both passbands, as demonstrated in Figure 17a. Similarly, by decreasing d_{l12} and d_{l21} from 3.8 mm to 2.2 mm, the bandwidths of the first and second passbands increase from 440 MHz to 520 MHz and from 1670 MHz to 1750 MHz, respectively. It is clearly seen that the bandwidth increases only from the right side in Figure 17b. Significant bandwidth enhancement and control can be achieved for both passbands as depicted in Figure 17.

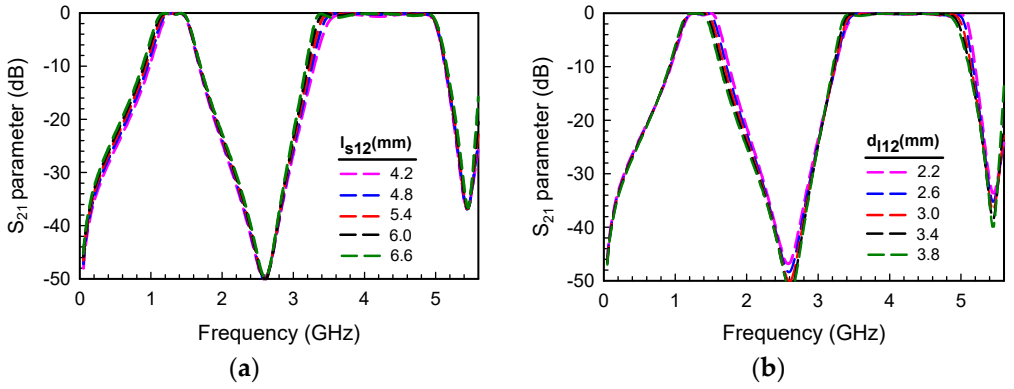

Figure 17. Bandwidth control of both passbands according to changes in (**a**) $l_{s12} = l_{s21}$, (**b**) $d_{l12} = d_{l21}$.

5. Experimental Study

Two-band bandpass filter prototypes have been fabricated on a Rogers RT6010LM substrate with a thickness of 1.27 mm and a relative dielectric constant of 10.2 for validation. The total surface areas of TBFSLR#1 and TBFSLR#2 are 26.0 mm × 9.0 mm and 24.4 mm × 16.8 mm, respectively. The fabricated prototypes and measured *S* parameters are shown in Figure 18. According to measured results, insertion losses are about 0.63 dB and 0.96 dB for the first and second passbands, respectively in TBFSLR#1. In TBFSLR#2, insertion losses are about 0.59 dB and 0.83 dB for the first and second passbands, respectively. TBFSLR#1 has a flat group delay while TBFSLR#2 provides higher selectivity. The differences between the measured and simulated results (in the bandwidth for the second

passband, especially) are thought to be due to manufacturing tolerances and measurement conditions. Table 2 shows a comparison between the proposed two-band bandpass filters and some filters described in the literature. As can be seen from the results shown in Table 2, generally, an equal number of modes are obtained in both passbands. The most distinctive difference between this study and studies in the literature is that this study allows two-band filter designs with Nth/2Nth order in the first/second passband, respectively. In addition, the proposed filters attract attention due to their low insertion loss and compact size as can be seen from Table 2.

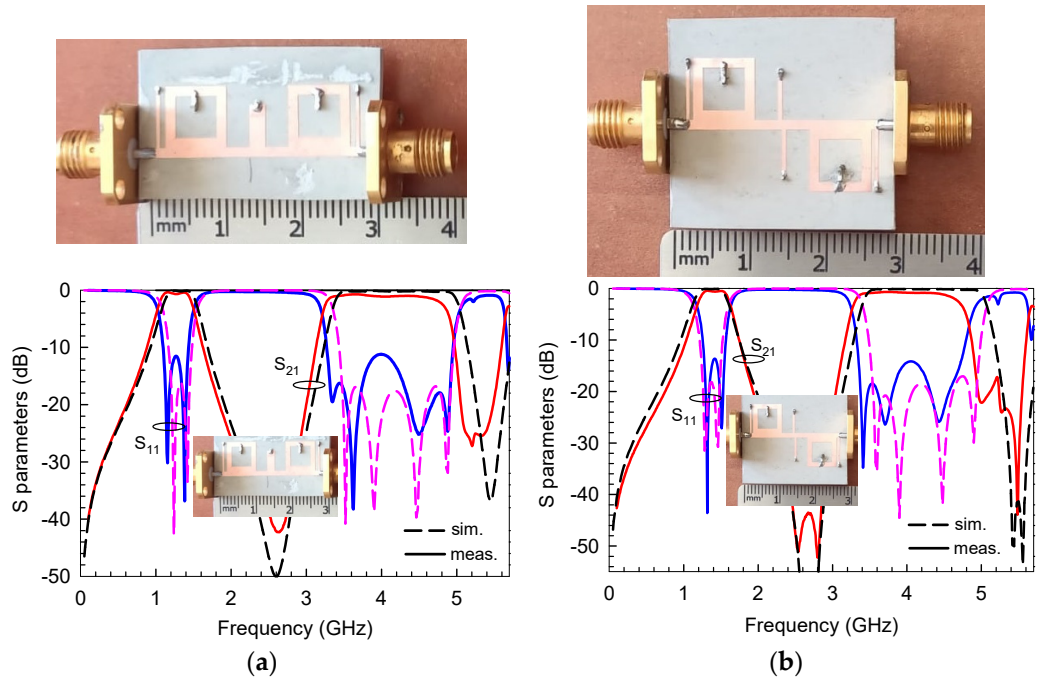

Figure 18. Comparison between the simulated and measured frequency responses of two-band BPFs with 2nd/4th order (**a**) TBFSLR#1 (**b**) TBFSLR#2.

Table 2. Comparison of the proposed two-band bandpass filters with similar filters in the literature.

Ref.	f_{01}/f_{02} (GHz)	3-dB FBW (%)	IL (dB)	Orders	Size ($\lambda_g \times \lambda_g$ *)
[3]	1.8/5.82	63/19	0.45/1.05	2/2	0.25 × 0.016
[5]	2.4/4.0	8/39	1.4/1.0	2/4	0.48 × 0.09
[7]	1.57/2.45	34.3/15.2	0.45/1.57	2/2	0.25 × 0.19
[8]	2.85/4.86	-	2.3/2.0	3/3	$0.16\lambda_g^2$
[12] (DBF#1)	1.1/5.26	65.6/30.7	1.2/1.05	2/2	0.28 × 0.12
[22]	2.12/3.91	15.3/5.5	0.92/2.11	2/2	0.24 × 0.18
[23]	3.78/4.82	11.3/10.7	1.38/1.82	2/2	0.16 × 0.31
[24]	2.4/5.2	51.9/23.3	0.3/0.7	2/3	0.28 × 0.20
[25]	2.4/5.2	14.8/12.9	1.43/1.34	2/2	0.30 × 0.15
This work (TBFSLR#1)	**1.28/4.03**	**34.8/40.2**	**0.63/0.96**	**2/4**	**0.27 × 0.093**
This work (TBFSLR#2)	**1.38/4.07**	**35.3/40.2**	**0.59/0.83**	**2/4**	**0.25 × 0.175**

* λ_g is the guided wavelength at the center frequency of the first passband.

6. Conclusions

In this study, a design concept for microstrip two-band filters that have first/second passbands with Nth/2Nth order is presented based on using square loop resonators and short-circuited stubs. A theoretical model is discussed by using the ABCD parameters to indicate the design procedure for the two-band filter having cascaded unit filter cells. The design method is demonstrated to be computationally efficient, and the computed results are in agreement with the simulated results. A reconfigurable filtering property in terms of transmission zeros has been accomplished, especially in the second passband, based on the placement of the cascade-connected unit filter cells in the horizontal axis. Two-band filter prototypes with 2nd/4th order in the first/second passband were fabricated and tested. According to measured results, insertion losses in the first/second passband are about 0.63 dB/0.96 dB and 0.59 dB/0.83 dB for TBFSLR#1 and TBFSLR#2, respectively. The total surface areas of TBFSLR#1 and TBFSLR#2 are 26.0 mm × 9.0 mm and 24.4 mm × 16.8 mm, respectively. The proposed bandpass filters exhibit low insertion loss, high selectivity or flat group delay, compact size, low radiation loss and flexible filtering characteristics. The designed filters are suitable for employment in sub-6 GHz 5G applications.

7. Patents

In the application process.

Author Contributions: Design and simulation, G.B.F.U. and P.Ö.Ö.; analysis, G.B.F.U. and P.Ö.Ö.; writing—original draft preparation, P.Ö.Ö. and G.B.F.U.; writing—review and editing, C.K.; supervision, C.K. All authors have read and agreed to the published version of the manuscript.

Funding: This work was supported by the Scientific and Technological Research Council of Turkey (TUBITAK) under Grant 120E101.

Conflicts of Interest: The authors declare no conflict of interest.

References

1. Liu, S.; Xu, J.; Xu, J.T. Compact dual-band bandpass filters using complementary split-ring resonators with closely spaced passbands. *Electron. Lett.* **2016**, *52*, 1312–1314. [CrossRef]
2. Tsai, L.C.; Hsue, C.W. Dual-band bandpass filters using equal length coupled-serial-shunted lines and Z-transform technique. *IEEE Trans. Microw. Theory Tech.* **2004**, *52*, 1111–1117. [CrossRef]
3. Li, D.; Zhang, Y.; Xu, K.; Li, L.W. Compact dual-wideband bandpass filter with good selectivity using side-coupled λ/4 shorted SIR. *J. Electromagn. Waves Appl.* **2015**, *29*, 69–79. [CrossRef]
4. Kaijun, S.; Jia, L.; Kezhou, P.; Jialin, H. Miniaturized cavity filters based on concentric dual-coaxial SIR. *J. Electromagn. Waves Appl.* **2022**, *36*, 2483–2495.
5. Weng, M.H.; Lan, S.W.; Chang, S.J.; Yang, R.Y. Design of Dual-Band Bandpass Filter with Simultaneous Narrow- and Wide-Bandwidth and a Wide Stopband. *IEEE Access* **2019**, *7*, 147694–147703. [CrossRef]
6. Zhang, Z.; Chu, Q.; Chen, F. Compact dual-band bandpass filters using open/short-circuited stub-loaded λ/4 resonators. *IEEE Microw. Wirel. Compon. Lett.* **2015**, *25*, 657–659. [CrossRef]
7. Yatao, P.; Lijun, Z.; Yongqing, L. A dual-mode dual-band bandpass filter using a tri-stubs loaded multimode resonator (TSLMR). *J. Electromagn. Waves Appl.* **2014**, *28*, 2067–2073.
8. Ge, J.; Wang, G. A dual-band filtering structure for highly selective reconfigurable bandpass filter and filtering balun. *Int. J. RF Microw. Comput. -Aided Eng.* **2022**, *32*, e23215. [CrossRef]
9. Ieu, W.; Zhang, D.; Zhou, D. High-selectivity dual-mode dual-band microstrip bandpass filter with multi-transmission zeros. *Electron. Lett.* **2017**, *53*, 482–484. [CrossRef]
10. Zhu, Y.; Li, J. Design of cross-coupled dual-band bandpass filter using stub-loaded open-loop resonators with different bandwidth ratios. *J. Electromagn. Waves Appl.* **2012**, *26*, 1492–1499. [CrossRef]
11. Gao, S.S.; Sun, S.; Li, J.L.; Yan, T. Compact dual-mode dual-band bandpass filter with inside-outside-reversed dual-ring topology. *Electron. Lett.* **2017**, *53*, 624–626. [CrossRef]
12. Karpuz, C.; Firat Unuk, G.B.; Ozturk Ozdemir, P. Novel design concept for microstrip dual band bandpass filter by using patch loaded resonator and short-circuited stub. In Proceedings of the IEEE Asia-Pacific Microwave Conference (APMC), Hong Kong, China, 8–11 December 2020; pp. 1024–1026.
13. Pozar, D.M. *Microwave Engineering*; John Wiley & Sons, Inc.: New York, NY, USA, 2011.
14. Hong, J.S.; Lancaster, M.J. *Microstrip Filters for RF/Microwave Applications*; Wiley: New York, NY, USA, 2001.

15. Eryılmaz, G.E.; Karpuz, C.; Gorur, A. Dual-mode microstrip filters with adjustable transmission zeros. *IET Microw. Antennas Propag.* **2008**, *2*, 839–847. [CrossRef]
16. Gorur, A. Description of coupling between degenerate modes of a dual-mode microstrip loop resonator using a novel perturbation arrangement and its dual-mode bandpass filter applications. *IEEE Trans. Microw. Theory Tech.* **2004**, *52*, 671–677. [CrossRef]
17. Alnahwi, F.M.; Al-Yasir, Y.I.A.; Abdulhameed, A.A.; Abdullah, A.S.; Abd-Alhameed, R.A. A Low-Cost Microwave Filter with Improved Passband and Stopband Characteristics Using Stub Loaded Multiple Mode Resonator for 5G Mid-Band Applications. *Electronics* **2021**, *10*, 450. [CrossRef]
18. Soroush, S.; Abdi, E. A lowpass filter implementation with an ultra sharp transition band and extended stopband bandwidth based on even-mode and odd-mode analysis of lumped circuits. *AEU Int. J. Electron. Commun.* **2022**, *149*, 154192. [CrossRef]
19. Quendo, C.; Rius, E.; Person, C. Narrow bandpass filters using dual-behavior resonators based on stepped-impedance stubs and different-length stubs. *IEEE Trans. Microw. Theory Tech.* **2004**, *52*, 1034–1044. [CrossRef]
20. Zakharov, A.; Litvintsev, S. Expanding functionality of dual-mode resonators and filters using nonuniform transmission line structural elements. *IEEE Trans. Circuits Syst. I Regul. Pap.* **2022**, *69*, 3124–3135. [CrossRef]
21. *EM User's Manual*; Sonnet Software Inc.: Liverpool, NY, USA, 2008.
22. Chen, H.; Chen, K.S.; Chen, X. Planar dual-mode dual-band bandpass filter using a modified rectangular split-loop resonator loaded by an open-circuited stub. *J. Electromagn. Waves Appl.* **2016**, *30*, 1964–1973. [CrossRef]
23. Wang, L.; Xiong, Y.; Gong, L.; Zhang, M.; Li, H.; Zhao, X.J. Design of dual-band bandpass filter with multiple transmission zeros using transversal signal interaction concepts. *IEEE Microw. Wirel. Compon. Lett.* **2019**, *26*, 32–34. [CrossRef]
24. Liang, G.; Chen, F.A. Compact dual-wideband bandpass filter based on open-/short-circuited stubs. *IEEE Access* **2020**, *8*, 20488–20492. [CrossRef]
25. Weng, M.H.; Huang, C.Y.; Dai, S.W.; Yang, R.Y. An Improved Stopband Dual-Band Filter Using Quad-Mode Stub-Loaded Resonators. *Electronics* **2021**, *10*, 142. [CrossRef]